

Localized states in coupled Cahn-Hilliard equations

TOBIAS FROHOFF-HÜLSMANN *

*Institut für Theoretische Physik, Westfälische Wilhelms-Universität Münster,
Wilhelm-Klemm-Str. 9, 48149 Münster, Germany*
Corresponding author: t.froh01@uni-muenster.de

UWE THIELE†

*Institut für Theoretische Physik, Westfälische Wilhelms-Universität Münster,
Wilhelm-Klemm-Str. 9, 48149 Münster, Germany*
*Center for Nonlinear Science (CeNoS), Westfälische Wilhelms-Universität Münster,
Corrensstr. 2, 48149 Münster, Germany*
u.thiele@uni-muenster.de

[Received on 28 October 2020]

The classical Cahn-Hilliard equation corresponds to a gradient dynamics model that describes phase decomposition in a binary mixture. In the spinodal region, an initially homogeneous state spontaneously decomposes via a large-scale instability into drop, hole or labyrinthine concentration patterns of a typical structure length followed by a continuously ongoing coarsening process. Here we consider coupled Cahn-Hilliard dynamics for two concentration fields and show that nonvariational (or active, or nonreciprocal) coupling may induce a small-scale (Turing) instability. At the corresponding primary bifurcation a branch of periodically patterned steady states emerges. Furthermore, there exist localized states that consist of patterned patches coexisting with a homogeneous background. The branches of steady parity-symmetric and -asymmetric localized states form a slanted homoclinic snaking structure typical for systems with a conservation law.

Keywords: Cahn-Hilliard models, localized states, slanted homoclinic snaking, conservation laws, Turing instability, nonreciprocal interaction

Homogeneous mixtures of different materials are often unstable and undergo phase separation (demixing or decomposition). Such processes are abundant in nature and technology where they occur for many multi-component materials ranging from solid alloys via soft gels and polymers to liquid mixtures [Langer, 1992; Bray, 1994; Gouyet et al., 2003; Onuki, 2002]. Quenching a homogeneous mixture into a parameter region where the uniform state is linearly unstable, phase separation occurs. In the initial stage, the mixture separates on a diffusive length scale into regions of one phase surrounded by the other phase, i.e., one obtains small clusters, drops or islands. A labyrinthine structure may also emerge. Subsequently, coarsening sets in, i.e., the mean structure size continuously increases in time until ultimately a single structure of system size prevails that corresponds to the global energy minimum [Langer, 1992; Bray, 1994].

The described behavior is typical for binary systems as well as for systems consisting of more components. The formation of stable patterns is normally not reported for such systems, in particular, they

*ORCID ID: 0000-0002-5589-9397

†homepage: <http://www.uwethiele.de>; ORCID ID: 0000-0001-7989-9271

are not known for the occurrence of localized states that consist of patterned patches coexisting with a homogeneous background. However, here we show that steady parity-symmetric and -asymmetric localized states can occur and show homoclinic snaking [Woods & Champneys, 1999; Burke & Knobloch, 2006] if phase separation in a multicomponent system is considered in an out-of-equilibrium setting typical for active media [Frohoff-Hülsmann et al., 2020].

The common model for phase separation was introduced by Cahn and Hilliard [Cahn & Hilliard, 1958; Cahn, 1965] and is widely studied as Cahn-Hilliard (CH) equation [Novick-Cohen, 1985; Langer, 1992; Bray, 1994; Onuki, 2002; Doi, 2013; Thiele et al., 2019]. In its classic form it can be presented as a mass-conserving gradient dynamics for a scalar order parameter field ϕ that corresponds to a scaled and shifted density [Cahn, 1965; Langer, 1992],

$$\partial_t \phi = \nabla \cdot \left[M \nabla \frac{\delta F[\phi]}{\delta \phi} \right]. \quad (0.1)$$

Here, M is a positive mobility constant and the underlying free energy functional is [Cahn & Hilliard, 1958]

$$F[\phi(\mathbf{x}, t)] = \int_V \left[\frac{\kappa}{2} |\nabla \phi|^2 + g(\phi) \right] d^n r, \quad (0.2)$$

with V being the considered volume. The first term in (0.2) penalizes interfaces ($\kappa \geq 0$) and $g(\phi)$ is a simple double-well potential that is specified later. Mobility functions $M(\phi)$ may also be considered [Kohn & Otto, 2002].

It is notable, that its character as a structure-forming but not pattern-forming model resulted in the remarkable feat that the CH equation avoided being mentioned in the monumental seminal review by Cross and Hohenberg on out-of-equilibrium pattern formation [Cross & Hohenberg, 1993]. In consequence, it has been slow to claim its place in the pattern formation community, in contrast to its prominence in soft matter and material science. However, it still made the classification of Halperin and Hohenberg [Hohenberg & Halperin, 1977] where it is known as “model B”.

Nevertheless, it is known for some time that the CH equation can show more intricate behavior if model amendments account for out-of-equilibrium driving forces. One example are laterally driven phase-separating systems that are described by the convective CH equation [Emmott & Bray, 1996; Golovin et al., 1998, 2001]. It corresponds to a CH equation with an additional Burgers-type convective term that breaks the gradient dynamics structure but is still mass-conserving. A recent numerical bifurcation study analyzes in detail how coarsening is suppressed by the lateral driving [Tseluiko et al., 2020].

The convective CH equation models phase separation and coarsening dynamics in an externally imposed gradient or flow as encountered in various processing technologies. However, phase separation is now also recognized as a widespread mechanism employed by biological cells for its inner organization [Berry et al., 2018]. Then, the out-of-equilibrium character of living cells may crucially amend main features of phase-separation, e.g., by coupling it to chemical reactions. Such processes are studied for a number of particular systems involving membranes and/or centrosomes. For instance, John and Bär investigate the evolution of lipid domains in the cell membrane with a four-field model consisting of reaction-diffusion equations for proteins and regulating enzymes coupled to a CH-type equation for the lipid distributions (model II in John & Bär [2005]). The resulting model can show slowed-down coarsening or the emergence of traveling waves instead of coarsening. Other examples are models for phase separation in ternary mixtures with chemical reactions [Tong & Yang, 2002; Okuzono & Ohta, 2003]. An active emulsion model for centrosome dynamics uses a reactive coupling of two CH equations [Zwicker et al., 2015; Weber et al., 2019]. In a related conceptual model, two CH equations are

coupled by a reactive coupling of different type [Schüler et al., 2014]. There, arrest of coarsening and oscillatory dynamics are described.

Beside its gradient dynamics structure, the other characteristic feature of the CH model is the mass-conserving character of the dynamics. The important role of conservation laws in pattern forming systems is increasingly recognized [Matthews & Cox, 2000; Cox, 2004; Winterbottom et al., 2005; Knobloch, 2016] but their role in many specific systems still necessitates a deeper understanding. The mentioned nonvariational systems of two coupled CH equations keep either none [Schüler et al., 2014] or only one [Zwicker et al., 2015] of the two conservation laws of the original uncoupled equations. This may partly explain the rather different reported behavior. However, no comparative study is available.¹

In contrast, we consider a system of two CH equations with variational and nonvariational coupling that both preserve the full mass conservation properties of the uncoupled equations. A similar system has very recently been considered by Saha et al. [2020] and You et al. [2020] for a restricted (non-generic) choice of parameters. For the general case, Frohoff-Hülsmann et al. [2020] analyzes the intricate linear behavior closely related to the classical Turing system of two coupled reaction-diffusion systems. They show that coarsening may be arrested or suppressed linearly or nonlinearly, and scrutinize the related bifurcation behavior. Here, we pursue the question whether homoclinic snaking of localized states can be found for this coupled CH system. Namely, section 1 introduces the model, sketches the numerical method and defines the employed solution measures. The subsequent section 2 sketches the temporal and spatial linear stability analyses of uniform steady states and discusses under which conditions the system can show a small-scale stationary instability, i.e., a Turing instability. Section 3 then numerically analyzes the bifurcation behavior focusing on the occurrence of localized states and time-periodic behavior within the snakes-and-ladders structures. Finally, a conclusion is given in section 4.

1. Model

The model consists of two linearly coupled CH equations in one spatial dimension. After nondimensionalisation the model reads

$$\begin{aligned}\frac{\partial \phi_1}{\partial t} &= \frac{1}{L^2} \frac{\partial^2}{\partial x^2} \left(-\frac{1}{L^2} \frac{\partial^2 \phi_1}{\partial x^2} + f'_1(\phi_1) - (\rho + \alpha) \phi_2 \right) \\ \frac{\partial \phi_2}{\partial t} &= \frac{Q}{L^2} \frac{\partial^2}{\partial x^2} \left(-\frac{\kappa}{L^2} \frac{\partial^2 \phi_2}{\partial x^2} + f'_2(\phi_2) - (\rho - \alpha) \phi_1 \right).\end{aligned}\tag{1.1}$$

with the double-well potentials

$$\begin{aligned}f_1 &= \frac{a}{2} \phi_1^2 + \frac{1}{4} \phi_1^4, \\ f_2 &= \frac{a + a_\Delta}{2} \phi_2^2 + \frac{1}{4} \phi_2^4.\end{aligned}\tag{1.2}$$

As the dynamics of both fields is mass conserving, at all times

$$\begin{aligned}\int dx \phi_1 &= \phi_0 \\ \int dx \phi_2 &= \phi_0 + \Delta \phi_0,\end{aligned}\tag{1.3}$$

¹Also multi-species reaction-diffusion systems with one or two conservation laws are discussed by a number of groups. For a brief overview see the introduction of Frohoff-Hülsmann et al. [2020].

where for simplicity we fix $\Delta\phi_0 = 0$ throughout the present work. Hence, ϕ_0 is the mean concentration of both fields. In the following we employ ϕ_0 as our main control parameter.

The single CH equation for ϕ_1 without coupling has a critical point at $a = 0$ (and $\phi_0 = 0$), i.e., decomposition can only occur for $a < 0$. Since the parameter a represents an effective temperature, a_Δ is the difference in critical temperatures of the uncoupled fields. Furthermore, κ is the relative rigidity of the uncoupled fields, L is the effective domain size. For details of the nondimensionalisation and the effective parameters see Frohoff-Hülsmann et al. [2020]. The linear coupling is composed of a symmetric, variational part of strength ρ and an asymmetric, nonvariational part of strength α . Without the asymmetric coupling, the model represents a gradient dynamics of form (0.1) and the two species attract [repel] each other for $\rho > 0$ [$\rho < 0$]. Such nonvariational couplings are sometimes called nonreciprocal coupling as they break Newton's third law [Ivlev et al., 2015].

We emphasize that the chosen nonvariational coupling ensures that both conservation laws remain valid. This implies, that it can not represent a chemical reaction between the components, but could still model the effective interaction of two conserved catalysts whose nonvariational coupling is mediated by reactions with other species that are not explicitly modeled. It could also be seen as a continuous predator-prey-type model of two potentially 'phase separating' species: e.g., for positive α species one would be attracted by species two while species two is repelled by species one, not unlike the attraction-repulsion scheme in Chen & Kolokolnikov [2014]. Similar models are investigated in Saha et al. [2020]; You et al. [2020], the small but significant differences are discussed in the conclusion of Frohoff-Hülsmann et al. [2020].

In section 3 we provide a fully nonlinear analysis of localized steady states in the form of a numerical bifurcation analysis. In particular, we study solutions of (1.1) with $\partial_t\phi_1 = \partial_t\phi_2 = 0$ applying pseudo-arclength continuation using the *Matlab* package *pde2path* [Uecker et al., 2014]. Solution branches are tracked in parameter space via tangential predictors and Newton correctors while varying the main control parameter ϕ_0 . To take the conservation of both fields into account we impose (1.3) as integral side conditions and introduce virtual source terms in (1.1) whose strengths act as further continuation parameters. They are automatically kept at zero during all continuation runs. Following the branches, we numerically calculate the linear stability of the corresponding states and detect bifurcations. This then allows us to switch branches and construct the entire bifurcation diagram. In general, we use the L^2 -norm

$$\|\delta\phi\| \equiv \sqrt{\int \sum_{i=1,2} (\phi_i - \phi_0)^2 dx} \quad (1.4)$$

as solution measure.

2. Linear Stability of homogeneous states

First, we analyze the linear stability of steady homogeneous states $\phi(x) = (\phi_1(x), \phi_2(x)) = (\phi_0, \phi_0) \equiv \phi_0$ employing the harmonic ansatz

$$\phi(x, t) = \phi_0 + \delta\tilde{\phi}e^{ikx + \lambda t} \quad (2.1)$$

Inserting (2.1) into Eqs. (1.1) and linearizing in $\delta \ll 1$ yields

$$\lambda\tilde{\phi} = -q^2 \begin{pmatrix} q^2 + f_1'' & -(\rho + \alpha) \\ -Q(\rho - \alpha) & Q(\kappa q^2 + f_2'') \end{pmatrix} \tilde{\phi} \equiv -q^2 \mathbf{B} \tilde{\phi}. \quad (2.2)$$

where the second derivatives f_1'' and f_2'' are evaluated at ϕ_0 , and $q = k/L$. Due to the conserved character of the dynamics any homogeneous state is a steady solution of Eqs. (1.1) and homogeneous perturbations, i.e. $k = 0$, always correspond to the neutral eigenvalue $\lambda = 0$. Introducing $\tilde{\lambda} = \lambda/q^2$, and defining the difference in squared coupling strengths $\Delta \equiv \alpha^2 - \rho^2$ gives

$$\tilde{\lambda}_{\pm} = \frac{1}{2} \left[-\text{tr}\mathbf{B} \pm \sqrt{(\text{tr}\mathbf{B})^2 - 4 \det\mathbf{B}} \right] \quad (2.3)$$

$$\text{with } \text{tr}\mathbf{B} = q^2(1 + Q\kappa) + f_1'' + Qf_2'' \quad \text{and} \\ \det\mathbf{B} = Q[q^2 + f_1''] [\kappa q^2 + f_2''] + Q\Delta.$$

These rescaled eigenvalues are qualitatively equal to those obtained for generic two-species reaction-diffusion system as investigated, e.g., by Turing [1952]. In consequence, the linear behavior is similar showing a number of different linear instabilities. In addition to the common large-scale stationary (Cahn-Hilliard) instability, the model also exhibits large-scale oscillatory (Hopf) and small-scale stationary (Turing) instabilities. For a detailed discussion of equivalences of the present parameters and parameters in the reaction-diffusion system, and an analysis of all occurring instabilities see Sec. III of Frohoff-Hülsmann et al. [2020]. Here, we exclusively focus on the pattern forming small-scale stationary instability. Treating $f_1''(\phi_0)$ as primary control parameter, its onset occurs at

$$f_1''^T = \frac{1}{\kappa} \left[f_2'' \mp 2\sqrt{\kappa\Delta} \right] \quad (2.4)$$

with critical wavenumber

$$q_c^2 = \frac{1}{\kappa} \left[\pm\sqrt{\kappa\Delta} - f_2'' \right] \quad (2.5)$$

where the upper [lower] sign refers to cases $\kappa > 1$ [$\kappa < 1$]. Applying our specific choices for f_1'' and f_2'' [Eqs. (1.2)] and using ϕ_0 as primary control parameter the onset of the Turing instability is at

$$\phi_0^T = \sqrt{\frac{\pm 2\sqrt{\kappa\Delta} - a(1 - \kappa) - a_{\Delta}}{3(1 - \kappa)}}. \quad (2.6)$$

Note that from now on, for simplicity we set $Q = 1$.

In particular, a Turing instability requires nonvariational coupling stronger than the variational one, i.e. $|\alpha| > |\rho|$, and unequal rigidities, i.e. $\kappa \neq 1$. The latter condition is equivalent to the condition of unequal diffusion constants in the classical reaction-diffusion system. Fig. 1 illustrates the small-scale linear instability showing three dispersion relations for different $|\phi_0|$. For $|\phi_0| > \phi_0^T$ all eigenvalues are negative (blue line), at the threshold $|\phi_0| = \phi_0^T$ the maximum touches the k -axis at $k = Lq_c$ (red line). Decreasing $|\phi_0|$ further, a band of unstable wavenumbers widens around Lq_c (green line). In all three cases, all eigenvalues are real and the second branch ($\lambda_-(k)$) is always below zero, hence not shown.

Next, we consider the spatial eigenvalues which give an indication at which parameters localized steady states can be expected. Thus, we consider the time-independent version of Eqs. (1.1) and apply the ansatz $\phi(x, t) = \phi_0 + \delta\tilde{\phi}e^{\beta x}$ where β is the spatial eigenvalue. Then the solvability condition, $\det B = 0$ (with $q^2 = -\beta^2$) gives the four spatial eigenvalues

$$\beta = \pm \sqrt{\frac{\kappa f_1'' + f_2'' \pm \sqrt{(\kappa f_1'' - f_2'')^2 - 4\kappa\Delta}}{2\kappa}} \quad (2.7)$$

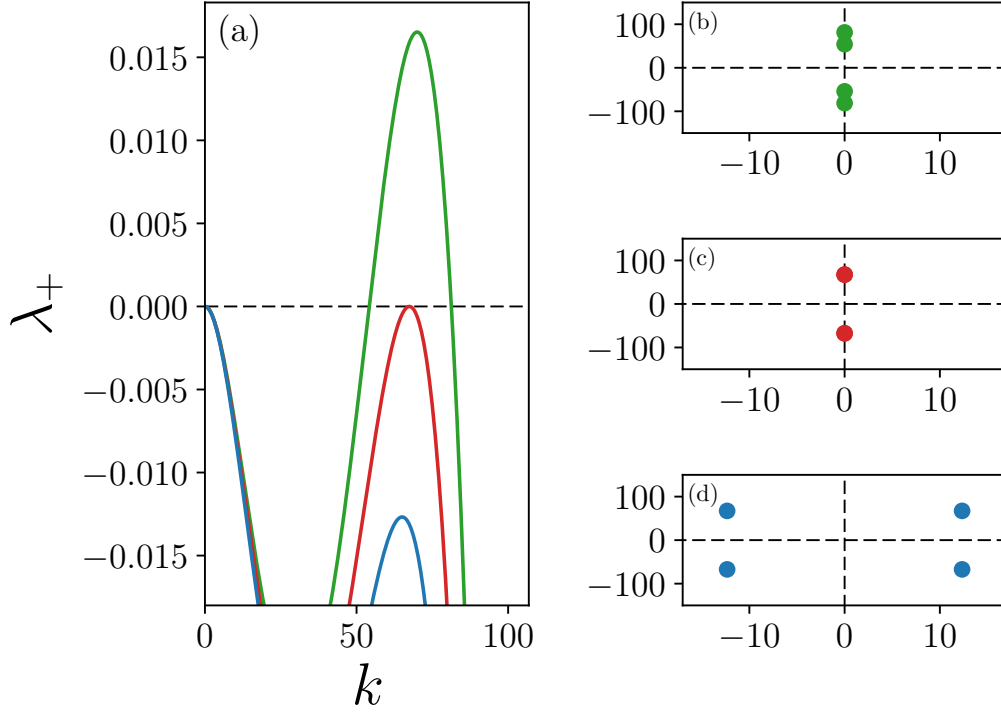


FIG. 1. The linear behavior near the onset of a small-scale (Turing) instability of the nonvariationally coupled CH equations. Panel (a) pictures three dispersion relations $\lambda_+(k)$: linearly stable case at $|\phi_0| = 0.22$ (blue line), neutrally stable case at $|\phi_0| = \phi_0^T \approx 0.211$ [Eq. (2.6), red line] and unstable case at $|\phi_0| = 0.2$ (green line). All eigenvalues are real. Panels (b)-(d) illustrate the corresponding motion of the four spatial eigenvalues in the complex plane at (b) $|\phi_0| = 0.2$, (c) $|\phi_0| \approx 0.211$, and (d) at $|\phi_0| = 0.22$. The remaining parameters are as in Fig. 2.

Their motion in the complex plane is depicted in Fig. 1 (b)-(d). At $f_1'' = f_1''^T$ [see panel (c)] they reflect the onset of linear instability, i.e., $\beta = \pm iq_c$ with double multiplicity. To study the vicinity of the Turing instability, we specify $f_1'' = f_1''^T + \varepsilon$ with $|\varepsilon| \ll 1$ and obtain

$$\begin{aligned} \beta &= \pm \sqrt{-q_c^2 \pm \sqrt{\frac{\varepsilon}{4\kappa}} \sqrt{\varepsilon\kappa + \text{sgn}(1-\kappa)4\sqrt{\kappa\Delta}} + \frac{\varepsilon}{2}} \\ &\approx \pm \left[iq_c \pm \frac{\sqrt{\text{sgn}(1-\kappa)}}{2q_c} \left(\frac{\Delta}{\kappa} \right)^{\frac{1}{4}} \sqrt{-\varepsilon} \right] \end{aligned} \quad (2.8)$$

with the sign-function $\text{sgn}(x)$. If $\kappa > 1$ [$\kappa < 1$] the homogeneous solution is Turing unstable for $\varepsilon < 0$ [$\varepsilon > 0$] and the spatial eigenvalues are purely imaginary, see panel (b), as expected for linearly unstable uniform states. Then, in the linearly stable case ($\varepsilon > 0$ [$\varepsilon < 0$]) the spatial eigenvalues form a quartet containing one pair of stable and one pair of unstable eigenvalues. That is, at the Turing threshold

the spatial eigenvalues switch from four complex ones to four imaginary ones. In consequence, an oscillatory approach to a uniform state is possible if the uniform state is linearly stable and the system is not too far away from the Turing threshold. All spatial eigenvalues become real for

$$|\phi_0| > \sqrt{\frac{1}{3(\kappa-1)} \left[a(1-\kappa) + a_\Delta - \sqrt{4\kappa\Delta} \right]}, \quad (2.9)$$

e.g., for the parameters of Fig. 2 for $|\phi_0| > 0.77$, i.e., far outside the shown range.

In summary, the obtained information on instability type and spatial eigenvalues allows us to conclude that localized states can emerge at $|\phi_0| \approx \phi_0^T$.

3. Snaking of localized states

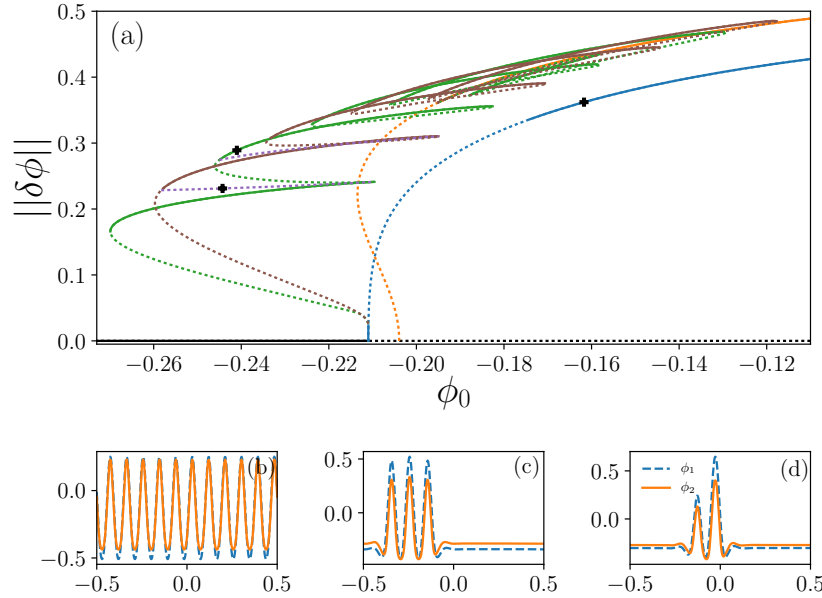


FIG. 2. (a) A typical bifurcation diagram for the nonvariationally coupled CH equations is presented focusing on branches of steady localized states. Shown is the L^2 -norm as a function of the mean density ϕ_0 at fixed $\alpha = 1.65$. Steady symmetric localized states with an even and an odd number of peaks are shown as brown and green lines, respectively. Also included are the two lowest branches of steady asymmetric localized states (purple dashed lines), the periodic steady states with $n = 11$ peaks (blue line) and $n = 9$ peaks (orange line), and the uniform state (black line). Solid and dashed lines indicate stable and unstable states, respectively. Panels (b) to (d) show example profiles at parameters marked by bold +-symbols in panel (a). The remaining parameters are $\kappa = 0.14$, $a = 1.25$, $a_\Delta = -1.9$, $\rho = 1.35$, and $\Delta\phi_0 = 0$. The domain size is $L = 20\pi$.

Having identified conditions for a Turing instability, we next investigate the resulting fully nonlinear behavior by addressing the bifurcation behavior of steady states. We use the common mean concentra-

tion ϕ_0 of the two fields as main control parameter (i.e., always $\Delta\phi_0 = 0$) and discuss the dependency of the bifurcation behavior on temperature a and on the strength of nonvariational coupling α . Our present choice $\Delta\phi_0 = 0$ results in the inversion symmetry $(\phi_i, \phi_0) \rightarrow (-\phi_i, -\phi_0)$. Hence, all bifurcation diagrams obtained here for $\phi_0 < 0$ can be reflected at $\phi_0 = 0$ to obtain the complete picture.

Fig. 2 (a) gives a typical bifurcation diagram and provides the main message of this work. It illustrates that the model features families of localized states that form the slanted (or tilted) homoclinic snaking structure (or slanted snakes-and-ladders structure) as usual for systems with a conservation law [Knobloch, 2016]. At the chosen values $a = 1.25$ and $\alpha = 1.65$, the uniform state is linearly stable for $|\phi_0| > \phi_0^T \approx 0.211$ [see Eq. (2.6)]. At $-\phi_0^T$ the first primary bifurcation occurs where a branch of 11-period steady states [blue line, cf. profile in Fig. 2 (b), called now “ $n = 11$ branch”] emerges supercritically. We also show the $n = 9$ branch of periodic states that bifurcates subcritically at slightly smaller $|\phi_0|$ (orange line). Further n -period branches emerge at $|\phi_0| < \phi_0^T$ (not shown). A discussion of periodic states, their stability and role in the arrest of coarsening is provided in Frohoff-Hülsmann et al. [2020].

The $n = 11$ branch of periodic states is first stable but soon loses its stability in a secondary pitchfork bifurcation where two branches of steady symmetric localized states emerge subcritically. They consist of localized states with an even (brown line) and odd number [green line, cf. profile in Fig. 2 (c)] of concentration peaks, respectively. The branches first continue towards larger $|\phi_0|$ before they turn in respective saddle-node bifurcations. Further such bifurcations follow and are related to the addition of pairs of peaks to the localized structure. When the domain is filled, both branches terminate subcritically on the $n = 9$ branch. In this way the latter branch gains stability. Whether the localized states end on the same branch from which they bifurcated off in the first place depends on the particular domain size. For further details on this finite size effect see Bergeon et al. [2008].

Furthermore, the slanted snakes-and-ladders structure contains the usual branches of unstable asymmetric states (purple lines) that connect the branches of symmetric states via two respective pitchfork bifurcations located in the vicinity of the saddle-node bifurcations. An example profile with two peaks (one of the first rung) is given in Fig. 2 (d). Note that all of these states are steady. In case of the asymmetric states this is remarkable for the present nonvariational model and will be further discussed elsewhere.

Next, we investigate the dependency of the slanted snakes-and-ladder structure when the effective temperature a is varied. Fig. 3 compares the behavior at four different values of a . The second lowest value, $a = 1.25$, is the structure already known from Fig. 2 (a). Increasing a shifts the entire structure toward larger ϕ_0 , and the neighboring saddle-node bifurcations on the snake move closer together, thereby narrowing the snaking structure. In consequence, these saddle-node bifurcations annihilate one pair after the other with each other in hysteresis bifurcations in a very similar manner as seen for variational phase-field-crystal models [Thiele et al., 2013; Holl et al., 2020]. At $a = 1.3$ most of the saddle-node bifurcations still exist, but the ones at largest peak number have already annihilated. Upon further increase in a , all saddle-node bifurcations vanish, and both secondary bifurcations become supercritical. Note that even without saddle-node bifurcations the two slanted branches still wiggle about each other and exchange stabilities via the branches of rung states that connect them. The resulting structure is termed smooth snaking. Ultimately, the two secondary bifurcations, where the localized states emerge, approach each other and annihilate. The final example in Fig. 3 at $a = 1.37$ is beyond this point and there only the branch of periodic states is left.

Considering again the $a = 1.25$ case of Fig. 2, we next discuss a decrease in a . Then, a transition from a supercritical to a subcritical primary bifurcation occurs at $a \approx 1.23$. Already at $a = 1.15$, the

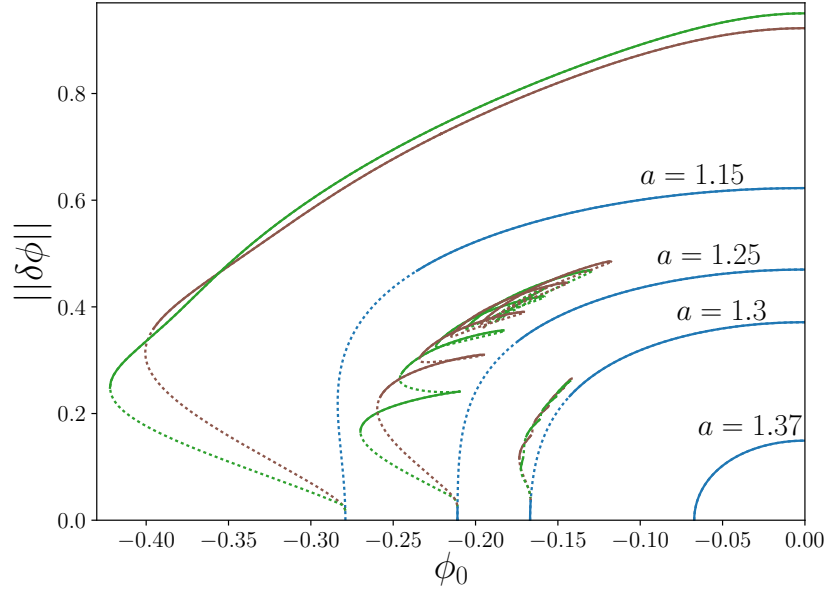


FIG. 3. The dependency of the entire slanted snakes-and-ladders structure on the effective temperature is shown. From left to right, the bifurcation structure as a function of ϕ_0 is shown for $a = 1.15, 1.25, 1.3$ and 1.37 . Line styles and remaining parameters are as in Fig. 2.

bifurcation structure has dramatically changed: As the width of the snaking region strongly increases with decreasing a , eventually, the rightmost saddle-node bifurcations of the snaking structure at negative ϕ_0 collide with their mirror images at positive ϕ_0 . Upon collision, they annihilate and the formerly continuous snakes-and-ladders structure is successively broken into more and more disconnected pieces. Only the two branches of one-peak localized states are still connected to the branch of steady periodic states and included in Fig. 2. The other branches of localized states are disconnected and not included in the figure.

Finally, we discuss qualitative changes in the bifurcation structure that occur when the nonvariational coupling strength $|\alpha|$ is varied. Using the example in Fig. 2 as reference case, we keep the variational coupling at $\rho = 1.35$ and increase $|\alpha|$. We also adjust a to stay in the parameter region of slanted snaking. The resulting bifurcation diagram for $\alpha = 1.78$ is presented in Fig. 4 (a) while panel (b) gives a corresponding dispersion relation for the homogeneous state at $\phi_0 = -0.3$: A band of stable oscillatory modes exists at wavenumbers to the left of the band of unstable stationary modes. Although, there is no direct influence on the linear behavior, we expect an impact on the fully nonlinear behavior.

Indeed, at $\alpha = 1.78$ beside the slanted homoclinic snaking structure of steady localized states with the usual sequences of saddle-node and pitchfork bifurcations, a number of Hopf bifurcations have appeared on the branches of steady symmetric and asymmetric localized states as well as on the branch of periodic steady states. They are marked by diamond symbols. One notes that the Hopf bifurcations predominantly occur near the left hand side saddle-node bifurcations of the snaking branches. Only

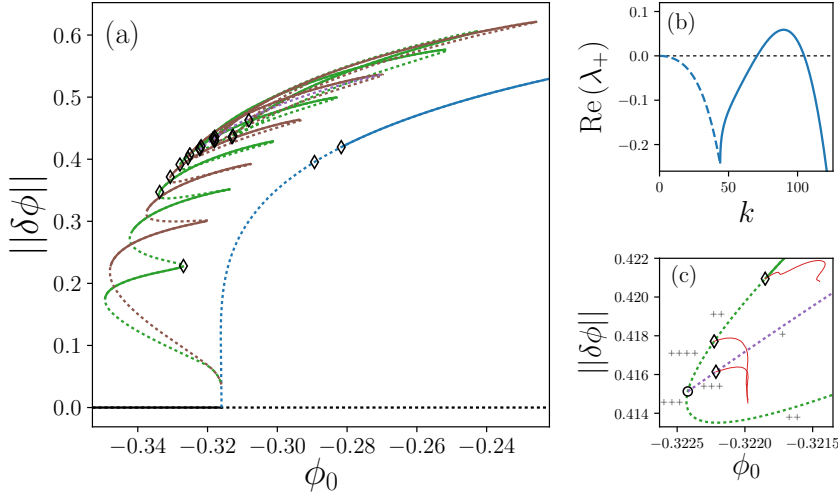


FIG. 4. (a) Bifurcation diagram in dependence of ϕ_0 illustrating the appearance of time-dependent behavior within the slanted snakes-and-ladder structure at high activity $\alpha = 1.78$, $a = 0.9$ and $\rho = 1.35$. The diamond symbols represent Hopf bifurcations where branches of time-periodic states emerge. The remaining line styles and parameters are as in Fig. 2. Panel (b) gives a dispersion relation at $\phi_0 = -0.3$ where solid [dashed] lines indicate real [complex] eigenvalues. Panel (c) magnifies a region of (a) near the emergence of the 8th rung state where Hopf bifurcations occur on branches of steady symmetric and asymmetric localized states. The number of unstable eigenvalues are indicated by “+”-symbols. Branches of time-periodic states are shown as thin red solid lines.

one of them is found on the right hand side, namely, near the lowest saddle-node bifurcation. On the left hand side, more and more such Hopf bifurcations occur the more filled the domain becomes. In particular, none exists near the lower four left saddle-node bifurcations, whereas one Hopf bifurcation is observed near each of the three next ones. Two such bifurcations appear near each of the four upper left saddle-node bifurcations. One example of the latter behavior is highlighted in Fig. 4 (c), which magnifies the region of panel (a) where the 8th rung state (purple line) emerges.

In Fig. 4 (c), the “+”-symbols represent the unstable eigenvalues and indicate how the appearance of Hopf bifurcations affects the character of saddle-node and pitchfork (circle symbol) bifurcation. Without Hopf bifurcations, the ascending snaking branch would first pass from two to one unstable eigenvalues at the saddle-node bifurcation, and then gain stability at the subcritical pitchfork bifurcation where the asymmetric rung state emerges. Now, however, at sufficiently large activity, saddle-node and (now supercritical) pitchfork bifurcation both further destabilize the branch such that it carries four unstable eigenvalues. These are subsequently stabilized via two Hopf bifurcations. Furthermore, the rung state emerges with three unstable eigenvalues, two of which are stabilized in another Hopf bifurcation.

Numerically continuing the emerging branches of time-periodic states is challenging, and can with present means only be achieved for parts of the branches. Nevertheless, the obtained behavior gives a consistent picture: The three obtained branches are shown in panel (c) as thin red solid lines. They represent standing waves and emerge subcritically, hence, are unstable. While the fully developed central peaks of the localized states show hardly any time dependence, the amplitudes of the outer two peaks oscillate strongly during a temporal period (not shown). First, we consider the two branches which

emerge from the symmetric steady states (green line). Standing waves on the left branch remain spatially symmetric at all times, i.e., the outer peaks oscillate in phase. In contrast, the standing waves on the right branch show broken reflection symmetry, i.e., the outer peaks oscillate in anti-phase. Corresponding to their symmetries, the former [latter] branch terminates in a homoclinic bifurcation on the lower, more unstable part of the branch of symmetric steady states [in a heteroclinic bifurcation on the branch of unstable asymmetric rung states]. The termination in a global bifurcation is indicated by a diverging time-period. This behavior is consistent with an appearance of these branches of time-periodic states in respective Bogdanov-Takens bifurcations at the saddle-node and the pitchfork bifurcation. The branch of asymmetric time-periodic states emerging at the Hopf bifurcation on the branch of asymmetric steady states also terminates on the branch of spatially symmetric steady states. In fact, we expect that it ends in the same homoclinic bifurcation as the other branch of time-periodic states, which is consistent with a simultaneous occurrence of the corresponding Hopf bifurcations. The branches of time-periodic states which emerge in the two Hopf bifurcations on the branch of the periodic steady states (blue line) terminate in homoclinic bifurcations on the unstable part of the same branch (not shown).

Note finally that at the considered parameters, there exist no drift-pitchfork bifurcations, that are a prevalent toward traveling localized states in other active media models like, e.g., the active phase-field-crystal model [Ophaus et al., 2018]. Following the approach of Ophaus et al. [2018] also here one may derive a condition, $0 = \int \phi_1^2 + \frac{\rho+\alpha}{\rho-\alpha} \phi_2^2 dx$, that indicates where drift bifurcations occur. However, for the shown branches of steady states, this condition is nowhere fulfilled.

4. Conclusion

We have explored a Cahn-Hilliard model consisting of two conservation laws with linear nonvariational (nonreciprocal) coupling. In contrast to expectations for Cahn-Hilliard models we have shown that above a critical activity the system can show a Turing instability and also exhibits slanted homoclinic snaking of localized structures, i.e., branches of symmetric and asymmetric localized states form a snakes-and-ladders structure.

Such features do not exist for the standard passive Cahn-Hilliard models. They describe decomposition into phase-separated structures that continuously coarse to approach thermodynamic equilibrium. Hence, it is the linear nonvariational coupling which dramatically changes the systems behavior. These findings are very much in line with recent studies of the intriguing impact of nonvariational or nonreciprocal interactions between order parameter fields [Menzel & Löwen, 2013; Schüler et al., 2014; Ophaus et al., 2018; Saha et al., 2020; You et al., 2020].

In particular, localized states do only exist because a strong nonvariational coupling can induce a short-scale instability in a Cahn-Hilliard system, normally characterized by large-scale instabilities. In consequence, stable periodic states are possible and coarsening can be entirely suppressed, as further investigated in Frohoff-Hülsmann et al. [2020]. Coarsening and its arrest in such a system is also investigated in Saha et al. [2020] by direct time simulation.

The emerging snakes-and-ladders structure is very similar to the one found in standard pattern forming systems with a conservation law [Knobloch, 2016], e.g., in the conserved Swift-Hohenberg (or phase-field-crystal) model [Thiele et al., 2013] and its active variants [Ophaus et al., 2018; Holl et al., 2020]. Correspondingly, we observe a similar change in behavior for decreasing temperature a . In particular, the transition from inexistent localized states, to smooth slanted snaking, to (standard) slanted snaking with saddle-node bifurcations and finally to broken snaking seems to be generic for localized states of conserved quantities.

However, in contrast to the variational case of a gradient dynamics where slanted snaking with the

mean concentration as control parameter is equivalent to vertically aligned snaking when the chemical potential is employed as control parameter [Thiele et al., 2013; Holl et al., 2020], for the present active system no such direct mapping can be expected. In consequence, the present system should be directly compared to its counterpart with nonconserved dynamics, namely, nonvariationally coupled Allen-Cahn equations.

Another crucial difference to passive models are time-periodic states that appear at even stronger activity where oscillatory instabilities and corresponding Hopf bifurcations occur on the snakes-and-ladders structure. Qualitatively, the onset of time-periodic behavior in the nonlinear regime can be related with the occurrence of a band of (stable) complex eigenvalues in the dispersion relation of the uniform state. However, this relation needs further investigation.

A limitation of our study is that we have only described localized states that exist for $\alpha > \rho$, however, first results show that localized states appear for $\alpha < -\rho$, as well. This is not surprising since the linear behavior is invariant w.r.t. the sign of α , hence, the occurrence of a small-scale instability is still valid. Rather surprising is a dramatic modification in the bifurcation structure of the localized states, that occurs when the sign of the activity is changed. This should be further investigated in future work.

Note, finally, that the asymmetric localized states that form the rung states of the snakes-and-ladders structure remain at rest even at strong activity. This is somewhat unexpected as asymmetric states in nonvariational models are normally expected to drift. However, such states are also found in a number of active PFC models [Ophaus et al., 2018; Holl et al., 2020]. This will be further analyzed and explained in a forthcoming publication.

Acknowledgment

We acknowledge frequent discussions with S.V. Gurevich, M.P. Holl and E. Knobloch, in particular, about impossible steady asymmetric states. The work is supported by the doctoral school “Active living fluids” funded by the German French University (Grant No. CDFA-01-14).

REFERENCES

- Bergeon, A., Burke, J., Knobloch, E. & Mercader, I. (2008) Eckhaus instability and homoclinic snaking. *Phys. Rev. E*, **78**, 046201.
- Berry, J., Brangwynne, C. P. & Haataja, M. (2018) Physical principles of intracellular organization via active and passive phase transitions. *Rep. Prog. Phys.*, **80**, 046601.
- Bray, A. J. (1994) Theory of phase-ordering kinetics. *Adv. Phys.*, **43**, 357–459.
- Burke, J. & Knobloch, E. (2006) Localized states in the generalized Swift-Hohenberg equation. *Phys. Rev. E*, **73**, 056211.
- Cahn, J. W. (1965) Phase separation by spinodal decomposition in isotropic systems. *J. Chem. Phys.*, **42**, 93–99.
- Cahn, J. W. & Hilliard, J. E. (1958) Free energy of a nonuniform system. I. Interfacial free energy. *J. Chem. Phys.*, **28**, 258–267.
- Chen, Y. X. & Kolokolnikov, T. (2014) A minimal model of predator-swarm interactions. *J. R. Soc. Interface*, **11**, 20131208.
- Cox, S. M. (2004) The envelope of a one-dimensional pattern in the presence of a conserved quantity. *Phys. Lett. A*, **333**, 91–101.
- Cross, M. C. & Hohenberg, P. C. (1993) Pattern formation out of equilibrium. *Rev. Mod. Phys.*, **65**, 851–1112.
- Doi, M. (2013) *Soft Matter Physics*. Oxford University Press, Oxford.

- Emmott, C. L. & Bray, A. J. (1996) Coarsening dynamics of a one-dimensional driven Cahn-Hilliard system. *Phys. Rev. E*, **54**, 4568–4575.
- Frohoff-Hülsmann, T., Wrembel, J. & Thiele, U. (2020) Linear and nonlinear suppression of coarsening in nonvariationally coupled Cahn-Hilliard equations. (preprint: <http://arxiv.org/abs/2009.14287>).
- Golovin, A. A., Davis, S. H. & Nepomnyashchy, A. A. (1998) A convective Cahn-Hilliard model for the formation of facets and corners in crystal growth. *Physica D*, **122**, 202–230.
- Golovin, A. A., Nepomnyashchy, A. A., Davis, S. H. & Zaks, M. A. (2001) Convective Cahn-Hilliard models: From coarsening to roughening. *Phys. Rev. Lett.*, **86**, 1550–1553.
- Gouyet, J. F., Plapp, M., Dieterich, W. & Maass, P. (2003) Description of far-from-equilibrium processes by mean-field lattice gas models. *Adv. Phys.*, **52**, 523–638.
- Hohenberg, P. C. & Halperin, B. I. (1977) Theory of dynamic critical phenomena. *Rev. Mod. Phys.*, **49**, 435–479.
- Holl, M. P., Archer, A. J., Gurevich, S. V., Knobloch, E., Ophaus, L. & Thiele, U. (2020) Localized states in passive and active phase-field-crystal models. (submitted).
- Ivlev, A. V., Bartnick, J., Heinen, M., Du, C. R., Nosenko, V. & Löwen, H. (2015) Statistical mechanics where Newton’s third law is broken. *Phys. Rev. X*, **5**, 011035.
- John, K. & Bär, M. (2005) Alternative mechanisms of structuring biomembranes: self-assembly versus self-organization. *Phys. Rev. Lett.*, **95**, 198101.
- Knobloch, E. (2016) Localized structures and front propagation in systems with a conservation law. *IMA J. Appl. Math.*, **81**(3), 457–487.
- Kohn, R. V. & Otto, F. (2002) Upper bounds on coarsening rates. *Commun. Math. Phys.*, **229**, 375–395.
- Langer, J. S. (1992) An introduction to the kinetics of first-order phase transitions. In Godrèche, C., editor, *Solids far from Equilibrium*, pages 297–363. Cambridge University Press.
- Matthews, P. C. & Cox, S. M. (2000) Pattern formation with a conservation law. *Nonlinearity*, **13**, 1293.
- Menzel, A. M. & Löwen, H. (2013) Traveling and resting crystals in active systems. *Phys. Rev. Lett.*, **110**, 055702.
- Novick-Cohen, A. (1985) The nonlinear Cahn - Hilliard equation: Transition from spinodal decomposition to nucleation behavior. *J. Stat. Phys.*, **38**, 707–723.
- Okuzono, T. & Ohta, T. (2003) Traveling waves in phase-separating reactive mixtures. *Phys. Rev. E*, **67**, 056211.
- Onuki, A. (2002) *Phase Transition Dynamics*. Cambridge University Press, Cambridge.
- Ophaus, L., Gurevich, S. & Thiele, U. (2018) Resting and Traveling Localized States in an Active Phase-Field-Crystal Model. *Phys. Rev. E*, **98**, 022608.
- Saha, S., Agudo-Canalejo, J. & Golestanian, R. (2020) Scalar Active Mixtures: The Non-Reciprocal Cahn-Hilliard Model. .
- Schüler, D., Alonso, S., Torcini, A. & Bär, M. (2014) Spatio-temporal dynamics induced by competing instabilities in two asymmetrically coupled nonlinear evolution equations. *Chaos*, **24**, 043142.
- Thiele, U., Archer, A. J., Robbins, M. J., Gomez, H. & Knobloch, E. (2013) Localized states in the conserved Swift-Hohenberg equation with cubic nonlinearity. *Phys. Rev. E*, **87**, 042915.
- Thiele, U., Frohoff-Hülsmann, T., Engelnkemper, S., Knobloch, E. & Archer, A. J. (2019) First order phase transitions and the thermodynamic limit. *New J. Phys.*, **21**, 123021.
- Tong, C. H. & Yang, Y. L. (2002) Phase-separation dynamics of a ternary mixture coupled with reversible chemical reaction. *J. Chem. Phys.*, **116**, 1519–1529.
- Tseluiko, D., Alesemi, M., Lin, T.-S. & Thiele, U. (2020) Effect of driving on coarsening dynamics in phase-separating systems. *Nonlinearity*, **33**, 4449–4483.
- Turing, A. M. (1952) The chemical basis of morphogenesis. *Philos. Trans. R. Soc. Lond. Ser. B-Biol. Sci.*, **237**, 37–72.
- Uecker, H., Wetzel, D. & Rademacher, J. D. M. (2014) pde2path - a Matlab package for continuation and bifurcation in 2D elliptic systems. *Numer. Math.-Theory Methods Appl.*, **7**, 58–106.
- Weber, C. A., Zwicker, D., Jülicher, F. & Lee, C. F. (2019) Physics of active emulsions. *Rep. Prog. Phys.*, **82**(6),

064601.

Winterbottom, D. M., Matthews, P. C. & Cox, S. M. (2005) Oscillatory pattern formation with a conserved quantity. *Nonlinearity*, **18**, 1031–1056.

Woods, P. D. & Champneys, A. R. (1999) Heteroclinic tangles and homoclinic snaking in the unfolding of a degenerate reversible Hamiltonian-Hopf bifurcation. *Physica D*, **129**, 147–170.

You, Z., Baskaran, A. & Marchetti, M. (2020) Nonreciprocity as a generic route to traveling states. *Proc. Natl. Acad. Sci.*, **117**, 19767 – 19772.

Zwicker, D., Hyman, A. A. & Jülicher, F. (2015) Suppression of Ostwald ripening in active emulsions. *Phys. Rev. E*, **92**, 012317.